Improvement of the IRAM 30–m Millimeter Wavelength Radio Telescope from Temperature Measurements and Finite Element Calculations

A. Greve, M. Bremer, J. Peñalver, P.Raffin, D. Morris, D. Broguire

***Abstract*— Millimeter wavelength radio telescopes built in a conventional way from steel and aluminum require elaborate thermal control to guarantee small structural deformations and good observational performance. We describe the temperature monitoring system of the IRAM 30–m telescope and the use of the temperature measurements in finite element calculations of structural deformations. These calculations reproduce the measured thermal deformations of the telescope with good precision and allow the investigation and localization of thermally important elements in the telescope structure. The data are used for the calculation of temperature induced main reflector surface deformations and of the associated actual beam pattern, and for prediction and real–time correction of the focus. Since the available finite element model does not include the Nasmyth focus cabin (and the concrete pedestal), the pointing cannot be predicted. The long–term investigation of the telescope's thermal behavior led to an improvement of the thermal control system and the performance of the telescope.**

***Index Terms*— Antennas mechanical factors, measurements.**

I. INTRODUCTION

THE IRAM 30–m diameter Cassegrain–Nasmyth telescope, supported on an alt–azimuth mount, is a homologous structure [1] designed for observations between ~ 3 mm (100 GHz) and ~ 1 mm (300 GHz) wavelength [2, 3]. The telescope is built in a conventional way from steel and aluminum (weight ~ 300 tons), and from the beginning it was evident that thermal deformations can be kept small only if the temperature of the telescope structure is controlled: *passively* by using complete insulation and white (TiO_2) paint on the outside; *actively* by using air–conditioned ventilation of the backup structure and fluid circulation around the subreflector supports (quadripod). The temperature of the backup structure and of the subreflector supports is slaved to a reference temperature measured in the upper part of the yoke, and under most operating conditions the temperature homogeneity of the backup structure and of the subreflector supports is $\sim 0.5\,^{o}$C (rms) [4]. There may, however, exist a temperature difference between the yoke, the backup structure, and the subreflector supports [4], primarily due to the different thermal time constants of these components. The yoke was until recently only passively controlled by insulation and paint, which in the design phase was considered to be sufficient because of its heavy weight, compactness, and estimated long thermal time constant, but also because of its use as temperature reference for the active thermal control system. This assumption seems today not to be fully correct.

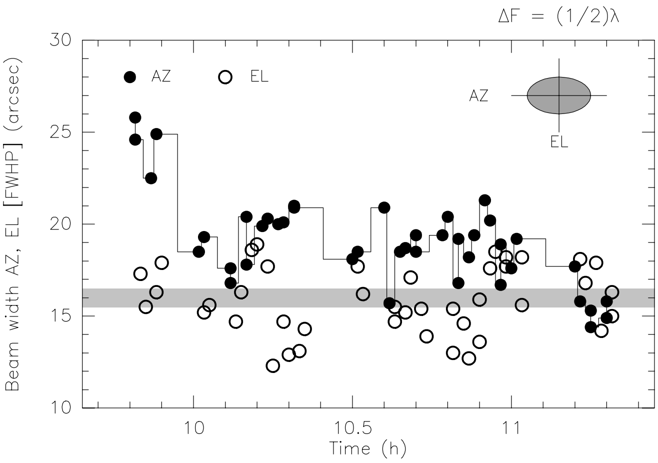

Fig. 1. Time evolution of the astigmatic beam of the IRAM 30–m telescope. For this mesurement the telescope was defocused (ΔF = (1/2) λ, at λ = 2 mm [150 GHz]) and the typical elliptical width of the astigmatic beam is shown. For a clean focused and defocused beam the width in AZ and EL direction is equal; the width of the focused beam is 16 arcsec (gray band).

The design, the operation, and the good performance of the thermal control of the IRAM 30–m telescope has been described earlier in detail [4, 5, 6]. However, during its 20 years of operation we have observed that the controlled telescope shows *transient residual* thermal deformations, which in scans across a radio source may appear as deformations of the beam pattern with associated changes in focus and pointing. Some of these effects have been described earlier [7, 8, 9]. To illustrate the situation, Fig. 1 shows the degradation of the beam pattern due to transient astigmatism, although during these measurements the telescope was correctly aligned, pointed, focused, and operated with thermal control. The observed beam degradation was exclusively due to transient thermal deformations since gravity (homology) acts in a known way and is considered in the pointing model [10], since the observations were made under calm and good atmospheric conditions, and since the beam degradation disappeared after ~ 2 hours. The long–term investigation of the thermal behavior

Manuscript received January 20, 2002; revised November 18, 2002.
The authors are, or were (P.R., D.M.), with the Institut de Radioastronomie Millimetrique (IRAM), 300 rue de la Piscine, 38406 St. Martin d'Heres, France.

has shown that astigmatism is the most frequent and prominent residual thermal deformation of the main reflector. The recent improvement of the thermal control system by installation of ventilation and heating of the counterweight sections of the yoke has reduced the residual thermal deformations.

The telescope operates within the original specifications [2, 3], and the work reported here was undertaken to improve its performance. We present the results to illustrate that modern measurement and computing techniques allow a good and real–time understanding and prediction of the thermal behavior of such a complex mechanical structure.

In order to investigate the thermal behavior of the telescope and to reduce the origin of similar beam degradations as shown in Fig. 1, we have installed 164 temperature sensors for detailed monitoring of the thermal state and for prediction of the temperature induced structural deformations from finite element (FE) calculations. We explain (Sect. II) the procedure to find for the temperature sensors the optimal location in the telescope structure; we discuss the accuracy of the thermal FE calculations; and we explain the use of a library (influence matrix) for economic calculations. We present (Sect. III) focus changes and deformations of the main reflector surface as calculated from measured temperature distributions and confirmed by radio measurements on the telescope. We present (Sect. IV) for two selected days the analysis of the thermal state of the telescope. When applied in a similar way to many other measurements, these analyses led to the understanding that thermal control of the yoke would reduce the residual temperature induced surface deformations of the main reflector. We explain (Sect. V) the improvement of the thermal control system and the improvement of the telescope performance. In the Summary we give recommendations for the installation of temperature sensors and the use of monitoring data in real–time predictions of temperature induced deformations and of their correction by direct or indirect means. [Similar thermal investigations of the OVRO 10–m open–air telescope and the JCMT 15–m astrodome–enclosed telescope are published in [11] and [12]].

II. TEMPERATURE SENSORS AND FINITE ELEMENT CALCULATIONS

We use a reconstructed FE model[1] of the IRAM 30–m telescope which consists of the yoke (YO, 180 tons), the backup structure (BUS, 100 tons), the four subreflector supports (SRS, each 5 tons), and the prime focus cabin (PFC) which holds the subreflector. A picture of the telescope is shown in Fig. 2 a; the steel structure contained in the FE model is shown in Fig. 2 b. This FE model reproduces the observed gravity induced gain–elevation variation of the main reflector with an accuracy[2] better than 10 % [13]. The FE model is, however, *incomplete* since it does not contain the azimuth bearing and the azimuth–rotating Nasmyth focus cabin, which supports the elevation bearings. The telescope rests on a concrete pedestal (Fig. 2 a) which is not considered in the model. With respect to the 9–parameter (P_i) pointing model applied on the telescope [10], the evident exclusion of the pedestal on which the azimuth bearing rests does not allow a FE determination of the tilt of the AZ axis (P_4, P_5); the exclusion of the Nasmyth focus cabin does not allow a FE determination of the tilt of the elevation axis (P_3). The temperature induced pointing variations can therefore not be predicted. However, the FE model is sufficient for the prediction of focus changes and variations of the main reflector surface shape under temperature loads, which is the main purpose of its use. The FE model allows the determination of the temperature induced variation of the main reflector collimation error (P_2).

The total number of FE nodes [(x,y,z) coordinates] of bar–, truss–, and plate–elements of the telescope model is 2348, with 1540 nodes used for the YO, 744 nodes for the BUS, 48 nodes for the SRS, and 16 nodes for the PFC. The FE thermal study of the telescope is based on 44 temperature sensors in the YO, 104 sensors in the BUS, and 2 sensors[3] per SRS. In total, approximately 7 % of the FE nodes are monitored by temperature sensors, in particular 3% of the nodes of the YO (primarily plate elements) and 14% of the BUS (primarily truss elements). The temperature sensors are fixed to the steel parts of the telescope, close to the selected FE nodes, and insulated against the environment. The accuracy of the temperature measurements is better than $\pm$ 0.05°C. The thermal state of the telescope is recorded every 5 minutes. The lay–out of the temperature monitoring system, its optimization, and examples of its use are also presented in [15].

Before we discuss the thermal behavior of the IRAM 30–m telescope, we explain (1) that the relatively small number of temperature sensors (156; on average 1 sensor per 2 tons of steel structure) provides a detailed and realistic picture of the actual temperature distribution throughout the FE–modelled telescope structure; and (2) that temperature measurements on the telescope and corresponding predictions from the FE model agree for representative thermal load cases, from which we conclude that the predictions can be applied with confidence for general use.

A. THE LOCATION OF THE TEMPERATURE SENSORS

The installation of temperature sensors at *all* FE nodes (**N** = 2348) is impossible. However, we have checked by numerical simulations that the measurement of temperatures of the selected subset of FE nodes [$\mathcal{T}_i$, i = 1,2,...,K = 156], and interpolation to the other FE nodes [T_i, i = 1,2,...,N–K] without sensor, provides the actual temperature distribution $[\mathbf{T}_N] = [\mathcal{T}_i]_K + [T_i]_{N-K}$ throughout the modelled telescope structure.

We selected for the temperature sensors in the BUS a homogeneous distribution throughout its volume. Simulations show [15] that this distribution of the temperature sensors approaches the optimal distribution with respect to the prediction of temperature induced surface deformations and of

[1]The original FE model, made by ARGE MAN KRUPP(now VERTEX), Germany, was lost, and a model was reconstructed from the telescope drawings.

[2]The accuracy is probably set by the precision of the radio measurements rather than the precision of the FE model or the mechanical behavior of the telescope structure [14].

[3]Today based on measurements of the temperature of the inflowing and outflowing thermal control liquid.

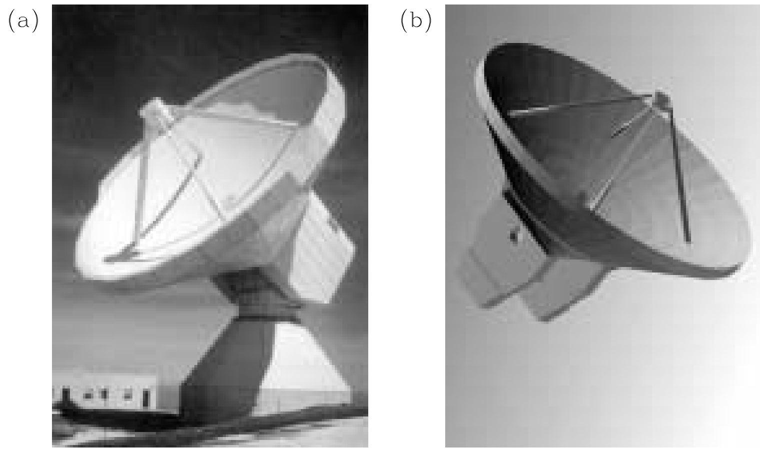

Fig. 2. The IRAM 30–m telescope (a) at Pico Veleta (Spain, 2 900 m altitude) and the steel part contained in the finite element model (b). The model does not contain the concrete pedestal and the central steel tower with AZ bearing, Nasmyth focus cabin, and EL bearings.

the associated collimation error. For the location of the temperature sensors in the YO we selected a set of thermally important FE nodes. The thermally important nodes produce per given temperature change the largest thermal deformation of the main reflector surface[4]. These nodes were deduced from FE calculations by subjecting each node to a certain thermal load (for instance a 1° C temperature difference with respect to its surrounding) and inspection of the associated surface deformation. The FE nodes and the temperature sensors selected in this way are shown in Fig. 3. [A similar approach to investigate thermally important nodes was used in a study of the alidade of the open–air Medicina 32–m telescope [16]].

B. INTERPOLATION OF TEMPERATURE MEASUREMENTS

In the FE calculations, each node must have an assigned temperature. The temperatures of the FE nodes without sensor $[\mathrm{T_i}]$ are obtained from interpolation of the measured temperatures $[\mathcal{T}_{\mathrm{i}}]$. The YO and the BUS are individual thermal units separated by a steel membrane (see Fig. 3)[5]; the interpolation of the temperatures is individually made for both structural components. For interpolation of the temperature of node [i], without sensor, from the surrounding nodes [j], with sensor, we use a weighting function of the distance $\mathrm{s(i,j)}^2 = (\vec{x}_\mathrm{i} - \vec{x}_\mathrm{j})^2$ between node $\vec{x}_\mathrm{i}$ and $\vec{x}_\mathrm{j}$ of the form

$$\mathrm{W(i,j)} = 1/[\mathrm{s(i,j)}^2 + \epsilon]^\mathrm{k} \qquad (1)$$

with ϵ = 0.1 [m] to avoid singularities. The interpolated temperature T(i) is

$$\mathrm{T(i)} = \sum\nolimits_{j,j\neq i} \mathcal{T}\mathrm{(j)\,W(i,j)} \,/ \sum\nolimits_{j,j\neq i} \mathrm{W(i,j)} \qquad (2)$$

We have checked the accuracy of the interpolation by selecting from adopted complete temperature distributions $[\mathbf{T}_\mathrm{N}] = [\mathcal{T}_\mathrm{i} + \mathrm{T_i}]$ the subsets of measured temperatures $[\mathcal{T}_\mathrm{i}]$ from which in turn the temperatures without sensors $[\mathrm{T_i}]'$ were obtained by interpolation, and from which the complete temperature distributions $[\mathbf{T}_\mathrm{N}]' = [\mathcal{T}_\mathrm{i} + \mathrm{T_i}']$ were reconstructed. We found that for the IRAM 30–m telescope the most accurate interpolation is obtained for k = 2 [Eq.(1)], and that the difference between the original complete set of temperatures $[\mathbf{T}_\mathrm{N}]$ and the interpolated temperatures $[\mathbf{T}_\mathrm{N}]'$ is $\sim$0.2–0.3° C (rms). The measured temperatures combined with the interpolated temperatures thus give a realistic picture of the thermal state of the FE–modelled telescope structure. We have checked the reliability of the interpolation in yet another way

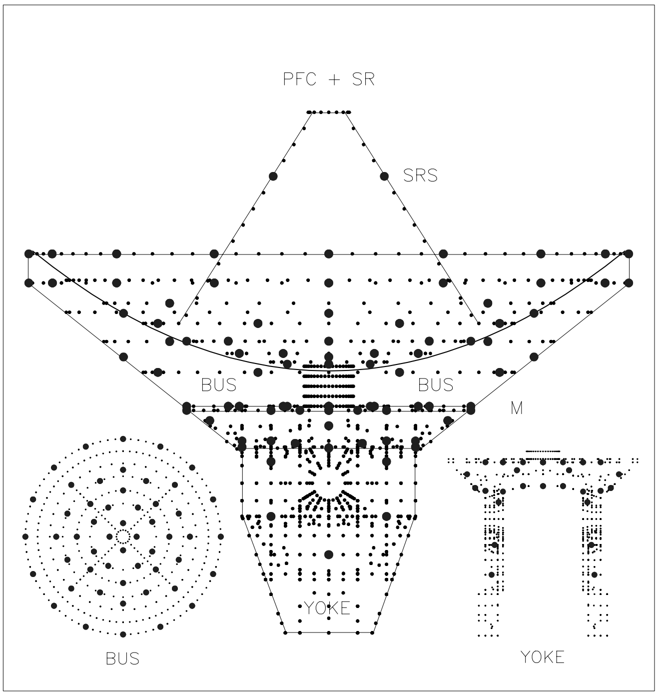

Fig. 3. Location of temperature sensors in the backup structure (BUS), the yoke (YO), and the subreflector supports (SRS). The small dots indicate the nodes of the FE model, the big dots the location of the temperature sensors. M is the membrane between the BUS and the YO. PFC + SR is the primary focus cabin and the subreflector.

[4]A similar selection can also be made for thermally important FE nodes which for instance produce the largest pointing error. This requires a complete FE model. The thermally important nodes of largest main reflector deformation may not coincide with the nodes of largest pointing error.

TABLE I

ACCURACY OF THE FE CALCULATIONS FOR RANDOM ERRORS IN THE TEMPERATURE MEASUREMENTS, LIMITED TO $|\Delta T_i| \leq 0.2^o$ C.

Parameter	Rms–value
FE Calculations	
Main reflector focus F	rmsΔF = 0.005 mm
Main reflector shift Δ(X,Y,Z)	rmsΔ(X,Y,Z) = 0.005 mm
Main reflector tilt $\psi_{\rm m(x,y)}$	rms$\Delta\psi_{\rm m(x,y)}$ = 0.5 arcsec
Surface precision σ	rms$\Delta\sigma$ = 0.003 mm
Subreflector shift Δ(U,V,W)	rmsΔ(U,V,W) = 0.005 mm
Subreflector tilt $\psi_{\rm s(x,y)}$	rms$\Delta\psi_{\rm s(x,y)}$ = 0.5 arcsec
Telescope Precision	
Homology deformations $\sigma_{\rm H}$ (zenith & horizon)	$\sigma_{\rm H}$ (rms) = 0.055 mm
Surface adjustment $\sigma_{\rm a}$	$\sigma_{\rm a}$ (rms) $\approx$ 0.055 mm
Focus determination	$\Delta\mathbf{z} \approx \pm 0.05 - 0.1$ mm
Pointing determination	ΔAZ, ΔEL $\approx \pm 1 - 2$ arcsec
Pointing model precision	$\sim 2 - 3$ arcsec (rms)

by calculating the structural deformations once for an adopted temperature distribution [$\mathbf{T}_{\rm N}$] of *all* FE nodes, and once for the full set of temperatures [$\mathcal{T}_{\rm i}$ + $\rm T_i$] = [$\mathbf{T}_{\rm N}$]' constructed from interpolation of the corresponding subset of temperatures [$\mathcal{T}_{\rm i}$]. The difference of the calculations, expressed as the difference of the deformations of all FE nodes calculated either way, is below 5 %.

C. ACCURACY OF THE FINITE ELEMENT CALCULATIONS

In numerical simulations we have investigated the influence of the accuracy of the temperature measurements on the result of the FE calculations. For this we constructed several complete temperature distributions [$\mathbf{T}_{\rm N}$] to which we added several (n) random error distributions [$\Delta\,\rm T_i]_n$, limited to $|\,\Delta \rm T_i| \leq 0.2^o$ C. For these distributions $[\mathbf{T}_{\rm N} + \Delta \rm T_i]_n$ we have calculated the corresponding rms–change of the main reflector focus [rmsΔF], of the main reflector vertex shift [rmsΔ(X,Y,Z)] and tilt [rms$\Delta(\psi_{\rm m(x,y)})$], of the main reflector surface precision [rms$\Delta\sigma$], and of the shift [rmsΔ(U,V,W)] and tilt [rms$\Delta(\psi_{\rm s(x,y)})$] of the subreflector. The results of these FE calculations are summarized in Table I, which also gives characteristic values of the current telescope precision. For an accuracy of the temperature measurements of $\sim 0.2^o$ C (rms), or better, the precision of the calculations is of the same order, or higher, than the precision with which these parameters can be measured on the telescope.

D. LIBRARY OF CALCULATED DEFORMATIONS (INFLUENCE MATRIX)

The investigation of thermal deformations of the main reflector surface and of the associated beam deformations is the main purpose of the study. The reflector surface of the IRAM 30–m telescope is defined by 260 FE nodes ($\rm k_{MR}$), the subreflector mount in the PFC is defined by 16 FE nodes ($\rm k_{SR}$). For the calculation of thermal deformations we have used the ANSYS^{TM} PC–FE package for static thermal loads. In order to speed up the calculations we have constructed a library (influence matrix) which contains for a 1^o C temperature change of each FE node [i; i = 1,2,...,2348 = **N**] the corresponding structural deformations $\vec{\delta}_{\rm R}(\rm k_{MR},i)$ [$\rm k_{MR}$ = 1,2,...,260] of the main reflector and the structural deformations $\vec{\delta}_{\rm RS}(\rm k_{RS},i)$ [$\rm k_{SR}$ = 1,2,...,16] of the subreflector mount. These calculations are combined in the influence matrix $\mathbf{M}_{\rm MR}$ of the main reflector (MR) and the influence matrix $\mathbf{M}_{\rm SR}$ of the subreflector, i.e.

$$\mathbf{M}_{\rm MR} = \begin{pmatrix} \vec{\delta}_{\rm MR}(1,1) & \cdots & \vec{\delta}_{\rm MR}(1,\mathbf{N}) \\ \vec{\delta}_{\rm MR}(2,1) & \cdots & \vec{\delta}_{\rm MR}(2,\mathbf{N}) \\ \cdots & \cdots & \cdots \\ \vec{\delta}_{\rm MR}(260,1) & \cdots & \vec{\delta}_{\rm MR}(260,\mathbf{N}) \end{pmatrix} \quad (3)$$

and similar for $\mathbf{M}_{\rm SR}$. The deformations $\vec{\Delta}_{\rm MR}$[k] of the reflector surface nodes [k, k = 1,...,260] for a specific thermal load case under consideration $\Delta \rm T_i$ (i = 1,2,..,**N**) are obtained from superposition of the individual deformations, i.e.

$$[\vec{\Delta}_{\rm MR}(1), \cdots, \vec{\Delta}_{\rm MR}(260)] = \mathbf{M}_{\rm MR} \times \begin{pmatrix} \Delta \rm T(1) \\ \Delta \rm T(2) \\ \cdots \\ \Delta \rm T(\mathbf{N}) \end{pmatrix} \quad (4)$$

The shift of the subreflector mount is obtained in a similar way and used in the calculation of the focus change. The library was verified against direct FE calculations of the same load cases. We find full agreement, as to be expected for the linear domain of thermal deformations. When using this library, the computation time is reduced by a factor of ~ 250 to a few seconds.

III. VERIFICATION OF THE THERMAL FINITE ELEMENT CALCULATIONS

We verified the thermal FE calculations against 39 GHz (7.7 mm) and 86 GHz (3.5 mm) focus measurements, and against a 180×180 pixel holography map of the main reflector surface made at 39 GHz using the geostationary satellite ITALSAT at 43^o elevation, where the homology deformations are negligible [13]. For these measurements we have taken the BUS out of thermal control and introduced 10 to 20 kW heat during several hours, in order to produce large structural deformations which produce easily measurable effects.

A. VERIFICATION OF CALCULATED FOCUS CHANGES

Figure 4 shows measured and calculated temperature induced primary focus (PF) and secondary focus (SF) variations. The measurements were made at 39 GHz (PF) and 86 GHz (SF) and Jupiter as radio source. The focus variation depends on the focal change (ΔF) and axial vertex shift (ΔZ) of the main reflector, and on the axial dilatation (ΔW) of the subreflector supports. In primary focus operation, the thermal deformations appear as a movement of the receiver with respect to the main reflector; in Cassegrain focus operation, the main reflector and subreflector appear to move with respect to the receiver in the Nasmyth focus cabin. The shift $\Delta\mathbf{z}$ of the receiver in primary focus observation, or of the subreflector in secondary focus observation, required to focus the thermally deformed telescope, is

$$\Delta\mathbf{z} = \Delta \rm F + \Delta Z - \Delta W \quad (5)$$

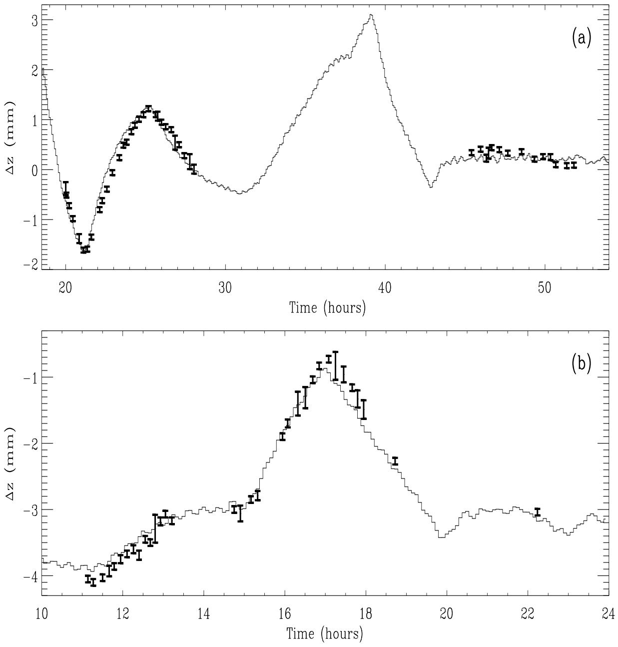

Fig. 4. Measured (symbols) and calculated (continuous line) focus corrections for observations (a) in prime focus [39 GHz], and (b) secondary focus [86 GHz]. The BUS was taken out of thermal control at the time t $\leq$ 43 h (a) and t $\leq$ 20 h (b). The figure shows also the small focus variations when the BUS and the subreflector supports are operated under thermal control.

with the quantities ΔF, ΔZ, and ΔW derived from the FE calculation of the corresponding temperature distribution. Within the errors of the measurement of $\delta(\Delta\mathbf{z}) \approx \pm 0.1$ mm, Fig. 4 shows good agreement between the measured and calculated temperature induced focus shifts. [Another example of calculated and measured focus changes, when the telescope settled to a stable temperature distribution after introducing into the BUS for two days ~ 500 kW for de–icing, is presented in [14]].

B. VERIFICATION OF CALCULATED MAIN REFLECTOR SURFACE DEFORMATIONS

The main reflector surface has an inherent shape with deformations [$\delta_{\rm a+H}$] due to panel alignment errors (a) and gravity induced (homology; H) deformations (see Table I). The temperature induced surface deformations [$\delta_{\rm T}$] are superimposed onto this inherent shape; the FE calculations predict the thermal deformations with respect to a perfect reflector. We verified the temperature induced deformations in a measurement with the BUS taken out of thermal control. From the corresponding holography measurement (made at primary focus) we derived the temperature induced surface deformations by subtracting from the map [$\delta_{\rm a+H+T}$], taken with the telescope in the disturbed thermal state, a map [$\delta_{\rm a+H}$] taken under very stable thermal conditions (with the thermal control working) representing the inherent shape. The resulting holography map [$\delta_{\rm T}$] = [$\delta_{\rm a+H+T}$] – [$\delta_{\rm a+H}$] of the temperature induced surface deformations is shown in Fig. 5 (top panel), while the main reflector surface deformations calculated from the measured temperature distribution is shown in Fig. 5 (lower panel). There exists good agreement in the amplitude and direction of the measured and calculated thermal surface deformations, being in this case primarily astigmatism. The comparison of the figures shows that the temperature induced deformations are predicted with the accuracy of 0.05 – 0.010 mm (which is comparable to the accuracy of the holography measurements).

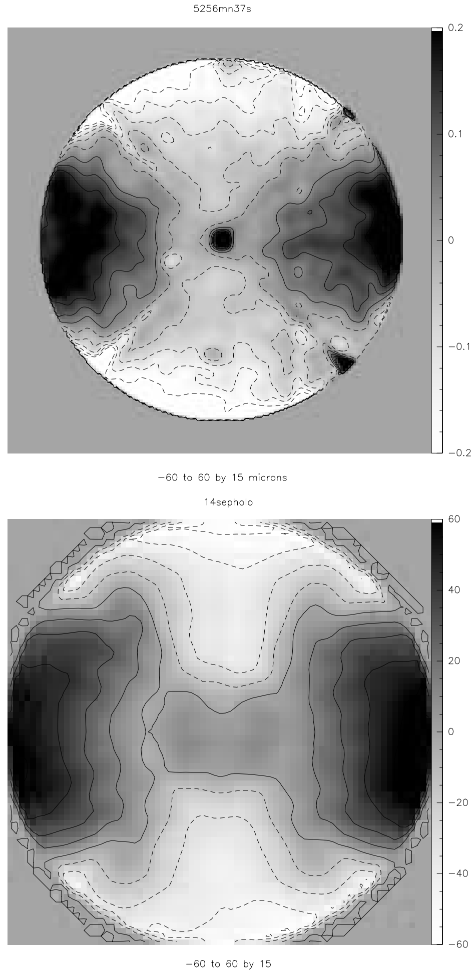

Fig. 5. Main reflector surface deformations derived from a 39 GHz holography measurement (top panel) and derived from finite element calculation for the corresponding thermal state of the telescope (lower panel). Contours in steps of 15 microns. The surface has a pronounced astigmatic deformation in elevation–azimuth (up–down, left–right) direction. During the measurement was the BUS thermally disturbed by introducing a large heat load.

IV. REPRESENTATIVE TEMPERATURE DISTRIBUTIONS (INITIAL THERMAL CONTROL)

The examples presented above demonstrate that it is possible to predict, with good accuracy, the temperature induced focus variations and main reflector surface deformations. In the following we present two examples which illustrate the thermal behavior of the IRAM 30–m telescope under initial thermal control (Period I, Table II) and normal observing conditions. Investigations of this kind led to an improvement of the thermal control system.

The temperature induced main reflector surface deformations consist of spatially small–scale random surface errors, which usually do not change the structure of the beam pattern and the focus and pointing, and of large–scale deformations, which may do so. Defining the reflector surface aperture by the normalized radial distance ρ ($0 \leq \rho \leq 1$) and angle θ ($0 \leq \theta \leq 2\pi$), we decomposed the calculated temperature induced surface deformations $\delta_{\rm T}(\rho,\theta)$ into large–scale contributions $\delta_{\rm Z}(\rho,\theta)$ represented by Zernike polynomials $\rm Z_{ij}(\rho,\theta)$ [20] and random errors $\delta_{\rm rd}(\rho,\theta)$, so that

$$\delta_{\rm T} = \delta_{\rm Z} + \delta_{\rm rd} = \sum\nolimits_{\rm i,j} \alpha_{\rm ij}\, {\rm Z_{ij}} + \delta_{\rm rd}$$

$$= \sum\nolimits_{\rm i,j} {\rm R_i}(\rho)[\alpha_{\rm AZ(ij)} \cos({\rm j}\theta) + \alpha_{\rm EL(ij)} \sin({\rm j}\theta)] + \delta_{\rm rd}(\rho,\theta) \quad (6)$$

with radial terms $\rm R_i(\rho)$, and the terms cos(jθ) for the AZ direction and sin(jθ) for the EL direction, respectively. The amplitude of the Zernike term (ij) is

$$\alpha_{\rm (ij)} = \sqrt{\alpha^2_{\rm AZ(ij)} + \alpha^2_{\rm EL(ij)}} \quad (5)$$

We subtracted from the temperature induced surface deformations $\delta_{\rm T}$ a best–fit parabolic surface, which can be realized by proper focusing. We obtain with respect to this best–fit surface the rms–value (root mean square) of the temperature induced surface deformations from

$$\sigma_{\rm T} = \sqrt{\sum\nolimits_{\rm n} \delta^2_{\rm T}/{\rm M}} \quad (7)$$

with M = 260 the number of surface elements considered in the FE calculations (see Sect. II.4).

We have investigated 4 000 hours of temperature recordings (summer through winter, 1996 – 1998) with the telescope operating under initial thermal control in order to obtain the statistics of the Zernike components. We find that the dominant Zernike polynomials, in order of importance, are astigmatism [L = 9 $\equiv$ (n,m) = (2,2) in the notation of Born & Wolf [20],[21]]

$$\delta_{2,2}(\rho,\theta) = \alpha_{2,2}\, \rho^2 \cos(2\,\theta), \quad (6)$$

4th order defocus [L = 3 $\equiv$ (n,m) = (4,6)]

$$\delta_{4,6}(\rho,\theta) = \alpha_{4,6}\, (6\,\rho^4 - 6\,\rho^2 + 1), \quad (7)$$

and 3rd order coma [L = 12 $\equiv$ (n,m) =(3,3)]

$$\delta_{3,3}(\rho,\theta) = \alpha_{3,3} \rho^3 \cos(3\,\theta). \quad (8)$$

The cumulative distributions of the amplitudes of these components are shown in Fig. 6. These dominant thermal deformations cannot be eliminated by a shift or tilt of the subreflector. We observe also that the Zernike polynomials of the thermal deformations are different from those of the gravity induced (homology) deformations [21].

In order to illustrate the initial thermal behavior of the telescope and arguments which led to a modification of the thermal control, we present a Day I (23 Jul 1998) when the telescope was in a homogeneous thermal state with negligible deformations, and a Day II (8 Oct 1998) when the temperature homogeneity was disturbed and a large transient astigmatic surface deformation occurred. We show in Fig. 7 for Day I ('good') and Day II ('poor') the calculated evolution of the temperature induced reflector surface deformations and the associated predicted (FFT) beam pattern at 1.3 mm (230 GHz) wavelength. Relatively small surface deformations and correspondingly clean beams are calculated for Day I [Fig. 7: I(a,b)], while during a substantial part of Day II [Fig. 7: II(a,b)] large astigmatic surface deformations and correspondingly deformed beams (at the – 18 dB level) are obtained. In [14] we have presented the beam pattern *measured* and correctly predicted for a similar condition as Day II.

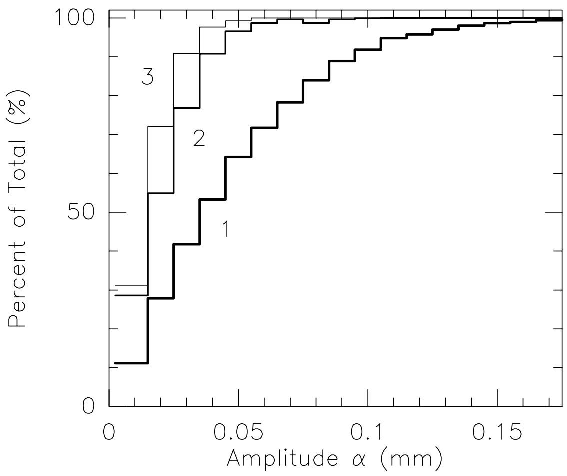

Fig. 6. Cumulative distribution of astigmatism (1), 4th order defocus (2), and 3rd order coma (3) of amplitude α, for telescope operation under initial thermal control (data of $\sim$ 1996 – 1998; Period I, Table II).

For the calculated thermal behavior of Day I and Day II we show in Fig. 8 the variation of the amplitudes $\alpha_{\rm AZ(ij)}$ and $\alpha_{\rm EL(ij)}$ of the Zernike polynomials (up to order (ij) $\equiv$ L = 20, [21]) throughout the day of investigation. On Day I, the temperature induced surface deformations are small, i.e. the rms–value is $\sigma_{\rm T} \approx$ 0.02 mm and the amplitude of all Zernike components is $|\,\alpha_{\rm L}\,| \leq$ 0.02 mm. During this day the temperature induced deformations are negligible with respect to the panel adjustment accuracy $\sigma_{\rm a}$ and the homology deformations $\sigma_{\rm H}$ (see Table I). On Day II, the rms–value is $\sigma_{\rm T} \approx$ 0.05 mm and the cosine–term astigmatism (at L = 9: AC) is the most important component of the temperature induced surface deformations with amplitude $|\,\alpha_{2,2}\,| \leq$ 0.12 mm. The sine–term astigmatism (at L = 25) is negligible, indicating that the axis of the astigmatism is oriented in AZ and EL direction, as it is always being observed (within $\sim \pm\, 20^{\rm o}$ deviation). Following Born & Wolf [20], an astigmatic surface deformation of amplitude $\alpha_9 \equiv \alpha_{2,2} \approx$ 0.12 mm has an effective quasi rms–value of $\sigma_{2,2} \approx (1/3)\, \alpha_{2,2} \approx$ 0.04 mm. This value is comparable to the rms–values $\sigma_{\rm a}$ and $\sigma_{\rm H}$ (see Table I), and thus contributes significantly to the beam degradation.

For a reduction of the dominant temperature induced astigmatism it is necessary to know its origin in the telescope structure. Supported by the experience that under initial thermal control also beam degradations are observed when the BUS has a homogeneous temperature distribution ($\sim$ 0.5 $^{\rm o}$C

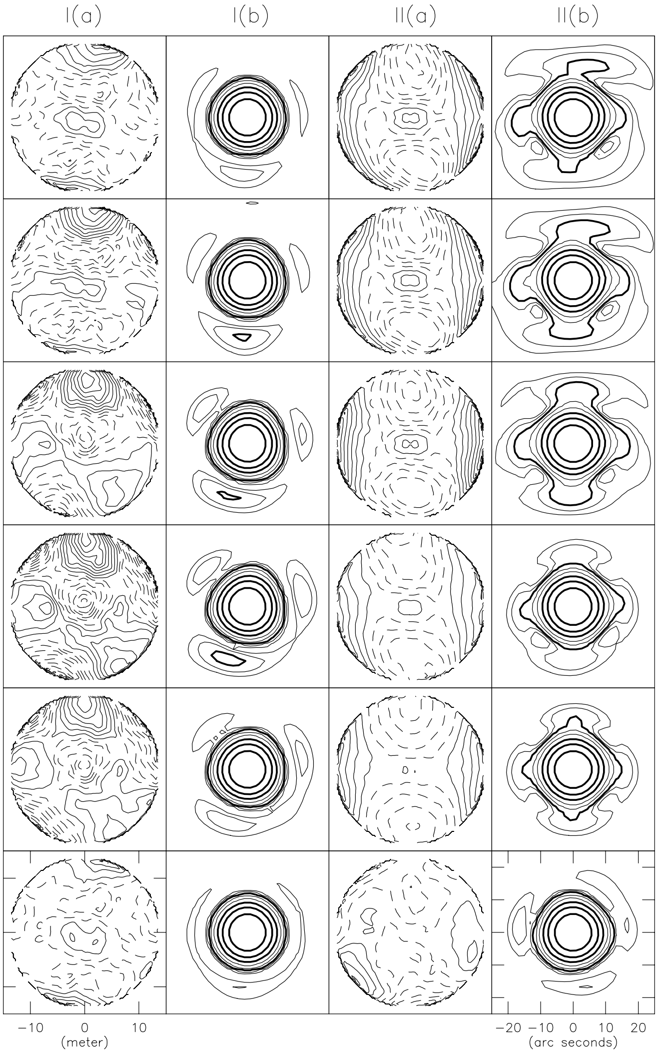

Fig. 7. Performance of the *initial thermal control system* (Period I, Table II). Temperature induced surface deformations of the main reflector and corresponding beam patterns at 1.3 mm (230 GHz) wavelength, for Day I (left) and Day II (right), as calculated from the corresponding temperature measurements, FE model calculations, and beam pattern calculations. Surface contour levels Day I: in steps of 0.015 mm, Day II: in steps of 0.04 mm. Contour levels of the beam patterns in steps of −3 dB (beam width), −6 dB, ..., −24 dB. From top to bottom: time steps of 6 h, starting at midnight.

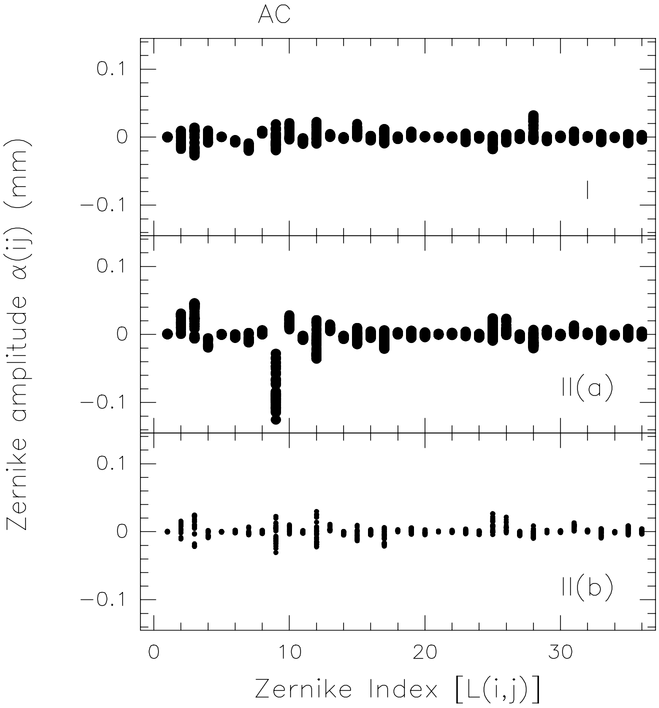

Fig. 8. Performance of the *initial thermal control system* (Period I, Table II). Amplitudes α(i,j) $\equiv$ α(L) (for L see [21]) of the Zernike polynomial components of the temperature induced main reflector surface deformations, for Day I and Day II (Fig. 7). The heavy dots in I, II (a) for a particular component L show the variation of the amplitude α(L) throughout the day. The panel II (a) displays the original data, panel II (b) shows the corresponding Zernike amplitudes α(L) with the YO assumed at a homogeneous temperature, i.e. the actually measured reference temperature.

rms) and is correctly slaved to the reference temperature of the YO (within $\sim 1^{\circ}$ C), and the experience that astigmatic deformations are small when a small temperature gradient inside the YO itself exists, we suspected that a temperature inhomogeneity of the YO is to a large extent responsible for the observed thermal deformations of the BUS, and in particular the dominant astigmatism of the BUS. To test this hypothesis we simulated for Day II the temperature induced surface deformations under the assumption that the YO has a *homogeneous* temperature. The calculation shows, as demonstrated in Fig. 8 [II(a) and II(b)], that the **in**homogeneous temperature distribution of the YO is to a large extent the origin of the astigmatism, and that the astigmatism would have been considerably smaller on Day II (α_9 = $\alpha_{2,2}$ $\approx$ 0.03 mm) if the YO would have had a homogeneous temperature. We concluded that the astigmatism is a 'print–through' of the thermally inhomogeneous and hence thermally deformed YO, even though the BUS and the SRS have a homogeneous temperature.

V. IMPROVEMENT OF THE THERMAL CONTROL SYSTEM

The study of the telescope has led to the following understanding of its behavior under initial thermal control:

– the temperature of the BUS agrees with the reference temperature of the YO (upper part) within $\sim 1^{\circ}$ C, while at the same time the temperature homogeneity of the BUS is $\sim 0.5^{\circ}$ C (rms) [4]. The telescope fulfills under this condition the original performance specification [2, 3] of a total surface accuracy of ≤ 0.10 mm and pointing accuracy of 2 – 3 arcsec, respectively.

– the main reflector has often an astigmatic surface deformation in the direction up–down, which is also the direction of the YO arms (see Fig. 2 (a)). The amplitude of the astigmatism is variable in time. For 10 – 15 % of the time the amplitude is 0.10 mm $\leq$ $\alpha_{2,2}$ (see Fig. 6) with an associated loss in main beam gain of $\sim$ 10 % at 1.3 mm wavelength. However, the astigmatism of the main reflector is negligible under the exceptional condition of an equal temperature of the BUS, the YO, and the counterweights.

– the temperature of the massive and compact counterweight areas, located in the lower part of the YO arms, is usually a

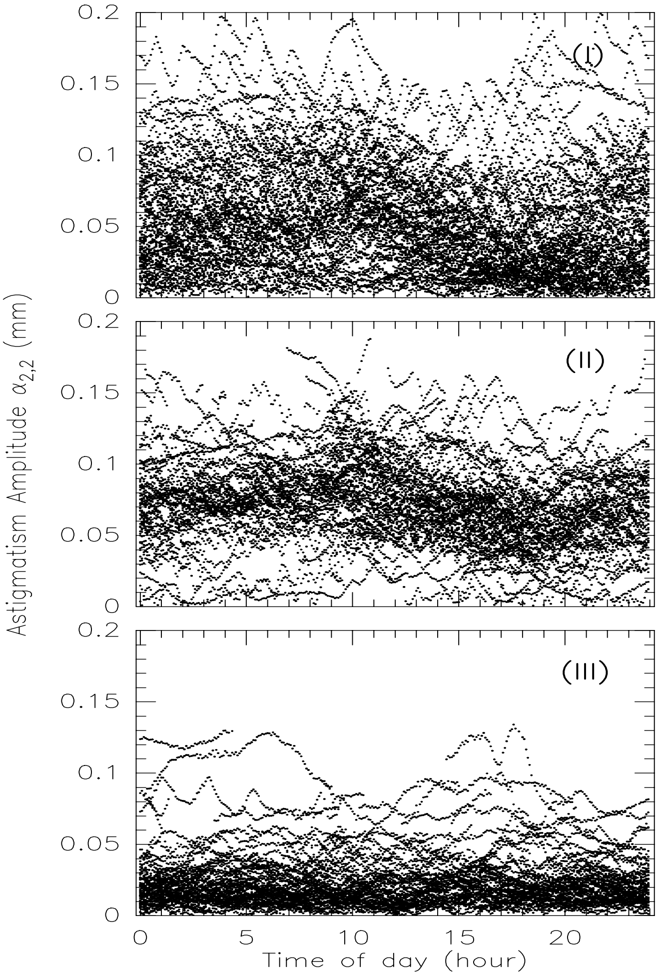

Fig. 9. Distribution of the astigmatism amplitude $\alpha_{2,2}$ throughout the time of day, (I) for the telescope operating under the initial thermal control system (ITC); (II) for the telescope operating under ITC and ventilation of the membrane area, (III) for the telescope operating under ITC and full ventilation/climatization of the YO (see Table II).

few degrees below the average temperature of the upper part of the YO (reference temperature) and the average temperature of the BUS, being slaved to the temperature of the YO. The higher temperature of the BUS and YO is partially due to heat released into the BUS during night time in order to counterbalance radiative losses toward the cool sky, and due to heat generated in the Nasmyth focus cabin and the cooling machinery, of which the hot air is exhausted near the upper part of the YO.

The occurrence of astigmatism during the time of initial thermal control (Period I) is shown in Fig. 9 (I), and summarized in Table II. As a first step toward improvement we have installed 4 ventilators (each 4 300 m^3 air circulation per hour) in the upper part of the YO, close to the membrane. As seen from Fig. 9 (II) and the data of Table II, with this operation (Period II) we obtained a reduction of the variation $\Delta_{2,2}$ (FWHP) of the astigmatism [expressed by the Gaussian distribution $\exp(-[(\alpha_{2,2} - <\alpha_{2,2}>)/\Delta_{2,2}]^2)$], but introduced a constant astigmatism of the order of $<\alpha_{2,2}> \approx 0.08$ mm. In September 2002 we have installed near the

TABLE II

REDUCTION OF THE MAIN REFLECTOR ASTIGMATISM.

Period / Year	$<\alpha_{2,2}>$ [mm]	$\Delta_{2,2}$ [mm]	Method of Thermal Control
I before Oct 1999	−0.03	0.060	initial thermal control (ITC)
II 1999 – 2002	−0.08	0.042	ITC + Membrane ventilation
III 2002 –	0	0.025	ITC + Membrane ventilation + Counterweight ventilation and heating

counterweights an additional servo–controlled ventilation and heating system[5]. This system circulates 4 300 m^3/h of air and supplies 6 kW (maximum) heating power at the lower part of each YO arm. Heating is applied to the counterweight areas whenever the temperature of the counterweights falls 0.15^o C below the reference temperature measured in the upper part of the YO. Ventilation is permanently applied in order to obtain a homogeneous temperature distribution throughout the counterweight areas. The limited time of operation (6 months, Period III) of the improved thermal control system has shown that the average temperature of the BUS, the YO, and the counterweights can be made and kept equal to within $\sim 1^o$ C under most circumstances. This is illustrated in Fig. 10 which shows the temperature homogeneity throughout the telescope structure (BUS, YO, and counterweight areas) for operation with the initial thermal control system and ventilation of the membrane area (Oct 2001) and operation with the fully improved thermal contral system (Oct 2002). Deviations of this temperature homegeneity occur during fast and large temperature changes of the ambient air to which the telescope components react differently according to their respective thermal time constant.

The reduction of the astigmatism by the improved thermal control is illustrated in Fig. 9. We compare in this figure especially the astigmatism calculated for the winter months (October to February) of the year 2001 – 2002 (Period II), when the initial thermal control and ventilation in the upper part of the YO close to the membrane was applied, and of the year 2002 – 2003 (Period III), when the improved thermal control system was working. The data displayed for period III refer to the time actually used for astronomical observations, thus omitting data taken during close–down time because of bad weather and de–icing conditions. A similar selection cannot be made for the period I and II; however, days with very large temperature variations throughout the telescope structure, which likely correspond to days without observations, have been omitted. The improvement of the telescope is evident. Currently, the quasi rms value of the astigmatism of $\sigma_{2,2} \approx (1/3)\,\alpha_{2,2} = (1/3)\,0.025$ mm = 0.008 mm (Table II) is negligible with respect to the panel alignment accuracy $\sigma_{\rm a}$ and the homology deformations $\sigma_{\rm H}$ (Table I).

The installation of an improved ventilation/climatization system is one way to improve the performance of the telescope. Since the surface shape of the main reflector is predicted with high precision, an active wavefront correction can be

[5] The active thermal control of the BUS consists of 5 ventilators allowing to move 63 000 m^3 internal air per hour. The climatization control consists of alternatively 30 kW heating or 20 kW cooling [4].

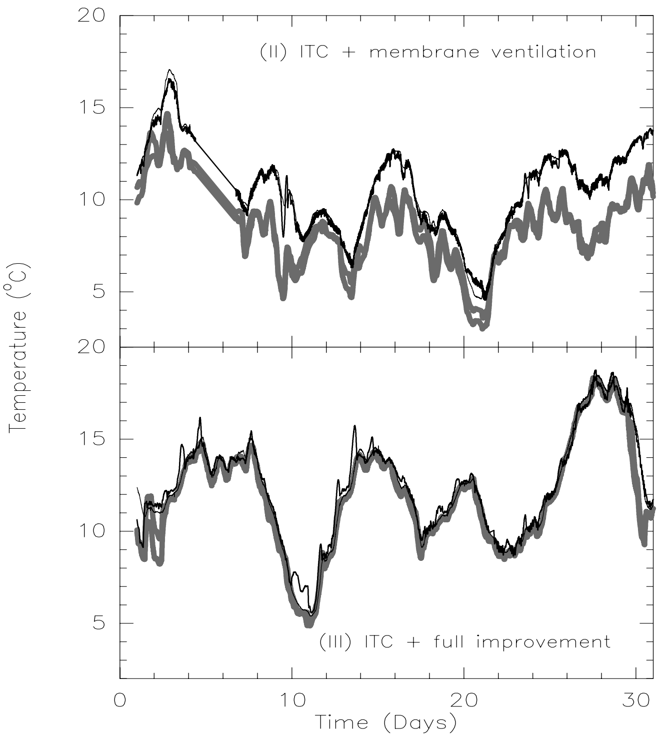

Fig. 10. Illustration of the temperature equality between the BUS and the YO (dark lines) and the left and right side counterweight areas (gray lines) for the ininital thermal control system and membrane ventilation (II) and the improved thermal control of the YO (full ventilation/climatization) (III) (see Table II).

envisaged as well. However, a large field of view requires an active (and expensive) subreflector, while an active (and inexpensive) Nasmyth mirror [21] allows only a good corretion of the on–axis beam.

VI. Summary

The investigation shows that it is possible to obtain a reliable and complete thermal picture of the FE–modelled part of the IRAM 30–m telescope from a relatively small number of temperature sensors, placed at especially selected positions, and interpolation of the measured temperatures. In this telescope we monitor the temperature of 7 % of the finite element nodes, so that each temperature sensor represents on average 2 tons of the modelled steel structure or ∼ 1/150 of the modelled weight. The location of the temperature sensors follows in the BUS a homogeneous distribution; in the YO the location is based on a finite element analysis which indicated the thermally most important nodes. The search for the location of important nodes with temperature sensor can be made either with respect to a prediction of the main reflector surface shape, as done here, or with respect to focus and pointing errors, or both. On other telescopes with a finite element model a similar strategy of the search for the location of temperature sensors can be applied.

With sensors installed in the afore mentioned way, the monitored temperatures can be used in a finite element calculation to obtain reliable values of the thermal deformations of the telescope structure, which can in turn be used for real–time prediction, and correction, of the thermal variation of the focus and on other telescopes probably also of the pointing. The derived temperature induced surface deformations can be used to calculate the deformed beam pattern and to quantify the corresponding radiometric performance of the telescope (gain variation, main beam degradation, increase in side lobe level, etc.). By actual measurements on the IRAM 30–m telescope we have verified the predictions based on this method. The use of the temperature influence matrix allows fast and real–time predictions.

When operating with the initial thermal control system, noticeable transient temperature induced surface deformations and associated beam degradations occur in the IRAM 30–m telescope, even though the backup structure and the subreflector supports are thermally stabilized to a high degree. The residual thermal deformations of the main reflector are primarily a print–through of thermal deformations of the, until recently, thermally non–controlled yoke. In future designs of (millimeter wavelength) radio telescopes it is recommended to investigate and, if neceessary, install a passive and/or active thermal control system throughout the *entire* steel/aluminum structure, but in particular also in the components which support the backup structure in order to avoid a print–through of deformations. The lay–out of the thermal control system can be based on exploratory studies of the *dynamic* thermal behavior of a telescope structure [5, 6], and by using finite element calculations as applied here for placement of the temperature sensors.

It remains a valid practice to slave the temperature of a telescope structure to its most massive part with the longest thermal time constant and hence the slowest temperature variation, as applied on the IRAM 30–m telescope. Evidently, as illustrated by the experience gathered on this telescope, this practice does not relax the condition of temperature homogeneity of this massive part (YO) of the structure.

While it is possible to obtain for the IRAM 30–m telescope a precise prediction of the focus correction, as experienced since long by using in an empirical way the temperature difference between the BUS and the YO [2], a similar statement cannot be made with respect to pointing corrections. The investigation of pointing requires a finite element model of the *complete* telescope structure and additional knowledge of other internal and external (thermal) influences, for instance of the foundation of the telescope (concrete pedestal), the tilt of the AZ[6] and EL axes, but also of the reliablity (stability) of the pointing model [10], the accuracy of refraction prediction, and the presence of anomalous refraction. The FE model of the IRAM 30–m telescope is not complete, which explains the encountered shortcomings.

In summary, in order to arrive at a successful project of temperature monitoring, prediction of thermal deformations of a telescope, and of thermal control if necessary, the following steps are recommended to be taken:

(1) a decision to predict temperature induced main reflector surface deformations, or the pointing and focus error, or both.

[6] Application of inclinometers on the 30–m telescope shows that the tilt of the AZ can be measured with high accuracy (∼ 0.5 arcsec) and considered in the pointing model in quasi real time [22].

(2) a search, based on the telescope's FE model, of the thermally most important nodes with respect to the question posed in (1), making use of an economic but sufficient number of temperature sensors, of the order of 150 to 250. While current FE models of telescope structures may contain of the order of 200 000 nodes, for thermal investigations a reduced model of $\sim 20\,000$ nodes may be consdidered which reliably reproduces the large model.

(3) construction of an interpolation method which allows the determination of the temperature of those FE nodes which have no temperature sensor; numerical checks of the interpolation method against straightforward thermal load cases (temperature gradients through the structure, random temperature distributions etc.); checks through numerical simulations of the adequacy of the number of measured temperatures.

(4) construction of a library (influence matrix) in order to avoid repetitive time consuming full FE model calculations.

(5) if possible, several conclusive experimental checks on the actual telescope structure, as explained here.

While the results presented in this paper may suggest the construction of a 'flobby' thermal telescope which is monitored and corrected in real–time, the experience indicates that a thermally well designed telescope, if necessary with thermal control, still provides significant advantages. We finally mention that the basic ideas of temperature monitoring and correction, as explained here, may eventually also be applied to wind induced deformations.

ACKNOWLEDGMENT

The project of understanding the thermal behavior of the IRAM 30–m telescope has taken many years. We appreciated the generous allocation of test time as well as the financial support throughout this project. We thank B. Lazareff (IRAM, France) for continued interest in this project, and critical review. We thank the operators and the astronomers on duty at Pico Veleta who have, in one or the other way, all taken part in this project. The data of Fig. 1 were obtained by S. Navarro (IRAM, Spain). The results of this project have been useful in the discussion of other (mm–wavelength) radio telescope projects (Sardinia telescope, ALMA).

REFERENCES

[1] S. von Hoerner, "Design of large steerable telescopes", *Astron. J.*, vol. 72, p. 35, 1967

[2] J.W.M. Baars, B.G. Hooghoudt, P.G. Mezger, and M. de Jonge, "The IRAM 30–m millimeter radio telescope on Pico Veleta, Spain", *Astron. Astrophys.*, vol. 175, p. 319, 1987

[3] J.W.M. Baars, A. Greve, H. Hein, D. Morris, J. Peñalver, and C. Thum, "Design parameters and measured performance of the IRAM 30–m millimeter radio telescope", *Proc. IEEE*, vol. 82, p. 687, 1994

[4] J.W.M. Baars, A. Greve, B.G. Hooghoudt, and J. Peñalver, "Thermal control of the IRAM 30–m millimeter radio telescope", *Astron. Astrophys.*, vol. 195, p. 364, 1988

[5] A. Greve, "Thermal design and thermal behaviour of telescope structures", IRAM, *Int. Report* 253, 1992

[6] A. Greve, M. Dan, and J. Peñalver, "Thermal behavior of millimeter wavelength radio telescopes", *IEEE Trans. Antennas Propagat.*, vol. AP–40, p. 1375, 1992

[7] A. Greve, B. LeFloch, D. Morris, H. Hein, and S. Navarro, " Astigmatism in reflector antennas: measurement and correction", *IEEE Trans. Antennas Propagat.*, vol. AP–42, p. 1345, 1994

[8] W.J. Altenhoff, "Workshop on pointing and pointing models", *MPIfR Techn. Ber. 78*, p. 39, p. 44, Bonn, March 1996

[9] A. Greve, C. Kramer, and W. Wild, "The beam pattern of the IRAM 30–m telescope", *Astron. Astrophys. Suppl.*, vol. 133, p. 271, 1998

[10] A. Greve, J.F. Panis, and C. Thum, "The pointing of the IRAM 30–m telescope", *Astron. Astrophys. Suppl.*, vol. 115, p. 379, 1996

[11] J.W. Lamb, and D.P. Woody," Thermal behavior of the Leighton 10–m antenna backing structure", *MMA Memo* 234, NRAO – USA, 1998

[12] F. Baas, "Temperature analysis of the JCMT telescope: comparison with early model calculations", *JCMT Techn. Report*, vol. 3, 1995

[13] A. Greve, R. Neri, and A. Sievers, "The gain–elevation correction of the IRAM 30–m telescope", *Astron. Astrophys. Suppl.*, vol. 132, p. 413, 1998

[14] A. Greve, "Radio telescopes in practice: Half–way towards end–to–end ?", *Proc. SPIE*, vol. 4757, p. 174, 2002

[15] M. Bremer, and J. Peñalver, "FE model based interpretation of telescope temperature variations", *Proc. SPIE*, vol. 4757, p. 186, 2002

[16] R. Ambrosini, G. Grueff, M. Morsiani, G. Maccaferri, P. Zacchiroli, and A. Orfei, "Analysis of the alidade temperature behaviour of the Medicina VLBI radiotelescope", *Astrophys. Space Sci.*, vol. 239, p. 247, 1996

[17] W.J. Altenhoff, J.W.M. Baars, D. Downes, and J.E. Wink, "Observations of anomalous refraction at radio wavelengths", *Astron. Astrophys.*, vol. 184, p. 381, 1987

[18] L. Olmi, "Systematic observations of anomalous refraction at millimeter wavelengths", *Astron. Astrophys.*, vol. 374, p. 348, 2001

[19] M.S. Zarghamee, and J. Antebi, "Surface accuracy of Cassegrain antennas", *IEEE Trans. Antennnas Propagat.*, vol. AP–33, p. 828, 1985

[20] M. Born, and E. Wolf, *"Principles of Optics",* Pergamon Press, UK, 1980

[21] A. Greve, J.W.M. Baars, J. Peñalver, and B. LeFloch, "Near focus active optics: An inexpensive method to improve millimeter wavelength radio telescopes", *Radio Science*, vol. 31., p. 1053, 1996

[22] J. Peñalver, U. Lisenfeld, and R. Mauersberger, "Pointing with the IRAM 30–m telescope", *Proc. SPIE*, vol. 4015, p. 632, 2001

Albert Greve see IEEE Trans Ant Propag. 1992, AP–40, 1375

Michael Bremer Biography text here.

Juan Panalver see IEEE Trans Ant Propag. 1992, AP–40, 1375

Phillipp Raffin Biography text here.

David Morris not available

Dominique Broguire Biography text here.